

An underdamped and delayed tri-stable model-based stochastic resonance

Yan-Fei Jin(靳艳飞), Hao-Tian Wang(王昊天), and Ting-Ting Zhang(张婷婷)
Citation: Chin. Phys. B, 2024, 33 (**1**): 010501. DOI: 10.1088/1674-1056/ad01a6
Journal homepage: http://cpb.iphy.ac.cn; http://iopscience.iop.org/cpb

What follows is a list of articles you may be interested in

Temperature-induced logical resonance in the Hodgkin-Huxley neuron

Haiyou Deng(邓海游), Rong Gui(桂容), and Yuangen Yao(姚元根)
Chin. Phys. B, 2023, 32 (**12**): 120501. DOI: 10.1088/1674-1056/accd49

Vibrational resonance in globally coupled bistable systems under the noise background

Jiangling Liu(刘江令), Chaorun Li(李朝润), Hailing Gao(高海玲), and Luchun Du(杜鲁春)
Chin. Phys. B, 2023, 32 (**7**): 070502. DOI: 10.1088/1674-1056/acc05f

Realizing reliable XOR logic operation via logical chaotic resonance in a triple-well potential system

Huamei Yang(杨华美) and Yuangen Yao(姚元根)
Chin. Phys. B, 2023, 32 (**2**): 020501. DOI: 10.1088/1674-1056/ac6945

Hyperparameter on-line learning of stochastic resonance based threshold networks

Weijin Li(李伟进), Yuhao Ren(任昱昊), and Fabing Duan(段法兵)
Chin. Phys. B, 2022, 31 (**8**): 080503. DOI: 10.1088/1674-1056/ac5886

Characteristics of piecewise linear symmetric tri-stable stochastic resonance system and its application under different noises

Gang Zhang(张刚), Yu-Jie Zeng(曾玉洁), and Zhong-Jun Jiang(蒋忠均)
Chin. Phys. B, 2022, 31 (**8**): 080502. DOI: 10.1088/1674-1056/ac588b

---

An underdamped and delayed tri-stable model-based stochastic resonance

Yan-Fei Jin(靳艳飞)†, Hao-Tian Wang(王昊天), and Ting-Ting Zhang(张婷婷)

Department of Mechanics, Beijing Institute of Technology, Beijing 100081, *China*

(Received 11 September 2023; revised manuscript received 7 October 2023; accepted manuscript online 10 October 2023)

Stochastic resonance (SR) is investigated in an underdamped tri-stable potential system driven by Gaussian colored noise and a periodic excitation, where both displacement and velocity time-delayed states feedback are considered. It is challenging to study SR in a second-order delayed multi-stable system analytically. In this paper, the improved energy envelope stochastic average method is developed to derive the analytical expressions of stationary probability density (SPD) and spectral amplification. The effects of noise intensity, damping coefficient, and time delay on SR are analyzed. The results show that the shapes of joint SPD can be adjusted to the desired structure by choosing the time delay and feedback gains. For fixed time delay, the SR peak is increased for negative displacement or velocity feedback gain. Meanwhile, the SR peak is decreased while the optimal noise intensity increases with increasing correlation time of noise. The Monte Carlo simulations (MCS) confirm the effectiveness of the theoretical results.

Keywords: stochastic resonance, underdamped tri-stable system, spectral amplification, time-delayed feedback

PACS: 05.40.–a, 02.50.–r **DOI:** 10.1088/1674-1056/ad01a6

1. Introduction

The ambient noise can play a constructive role in the output of the nonlinear system under some conditions. The benefits of noise and nonlinearity lead to the classical stochastic resonance (SR) phenomenon.[1] It is known that the SR has been widely studied theoretically, numerically and experimentally in many fields over the past decades.[2–4] However, most SR studies focus on the first-order dynamical model describing overdamped motions, in which the inertia term is ignored for simple of theoretical analysis. In practice, many systems generally need to be described as the second-order underdamped dynamical models, where the damping coefficient plays an important role in the SR effect.[5–11] For example, it is shown that a specific damping can generate the largest enhancement in SR under Gaussian white noises[5] or trichotomous noises[6] in the coupled underdamped bi-stable systems. The non-monotonic dependence of SR measures, such as SNR and spectral amplification, on damping parameter is found in an underdamped bi-stable system driven by noise and different harmonic signals.[7,8] For the underdamped periodic potential system,[9–11] the average input energy is maximized with the proper damping parameter. Yet it is a fact that the consideration of inertia term leads to the difficulty in theoretical analysis of SR. It is thus necessary to develop some new methods to deal with the SR theoretical derivation of the second-order or high-dimensional dynamical systems.

Multi-stability refers to the coexistence of multiple stable equilibrium states in nonlinear dynamical systems, which has been observed in many mechanical systems such as multi-stable energy harvesters,[12,13] nonlinear vibrational isolators,[14] and multi-stable inflatable origami structures.[15] When noise is considered in multi-stable systems, some interesting phenomena such as noise-induced resonances,[16,17] attractor preference,[18] and attractor hopping[19] spring up. Especially, the study of SR in multi-stable systems has attracted widely attentions.[20–26] For example, Nicolis *et al.*[20,21] analyzed the phenomenon of SR in multi-stable systems through the linear response and information entropy. Xu and Jin *et al.*[22,23] studied the noise-induced resonances in the Josephson junction and triple-well potential respectively, where the constructive effects of trichotomous noises and friction memory are explored. Zhang *et al.*[24] studied the logical SR induced by additive or multiplicative colored noise in the triple-well potential systems. Arathi *et al.*[25] reported that signal-to-noise ratio (SNR) can attain its maximum in the triple-well potential with a uniform depth. Jin *et al.*[26] studied SR and mean-first passage time of a quad-stable potential, which is applied to the fault diagnosis of inner and outer race bearing.

The time-delayed state feedback control is one of feasible methods of controlling unstable and chaotic motions by designing feedback gains and time delays.[27–29] However, the infinite dimensions of the solution space produce a hard problem to the theoretical treatment of stochastic delay differential equations (SDDEs). Some approaches such as the approximate Fokker–Planck equation[30] and the extended semi-discretization method[31] have been proposed to deal with SDDEs. Moreover, SR has been investigated in the dynamical system with time delay.[32–36] Tsimring *et al.*[32] proposed

†Corresponding author. E-mail: jinyf@bit.edu.cn

© 2024 Chinese Physical Society and IOP Publishing Ltd

the SR theory of a delayed bi-stable system under the two-state system approximation. Jin *et al.*[33,34] studied the noise-induced resonances in the delayed bi-stable and tri-stable systems driven by correlated additive and multiplicative noises. Xu *et al.*[35] found the correlation between the multiplicative and additive noises can induce stochastic multi-resonance phenomenon and noise-enhanced stability in a delayed triple-well potential. To the knowledge of authors, less attention has been paid to the SR in a second-order tri-stable system with time-delayed feedback control and colored noise.

The main purpose of this study is to derive the analytical expression of the spectral amplification and analyze the SR in an underdamped tri-stable system with both displacement and velocity delayed states feedback and colored noise. In Section 2, an underdamped tri-stable system with displacement and velocity delayed states feedback is modeled, which is driven by colored noise and a periodic signal. The stationary probability density (SPD) is obtained analytically by using the improved energy envelope stochastic average method. In Section 3, the analytical expression of the spectral amplification is derived to describe the SR phenomenon. The effects of noise intensity, damping coefficient and time delay on SR are discussed. Finally, some conclusions are drawn in Section 4.

2. An underdamped tri-stable system with delayed state feedback

In this study, the system of concern is an underdamped Brownian particle in a tri-stable potential with the displacement and velocity delayed states feedback. The corresponding Langevin equation is governed by

$$\ddot{x}+\gamma\dot{x}+\frac{\mathrm{d}U_0(x)}{\mathrm{d}x}=\beta x_\tau+\nu\dot{x}_\tau+\varepsilon\cos(\omega t)+\eta(t), \quad (1)$$

where $x_\tau=x(t-\tau)$, $\dot{x}_\tau=\dot{x}(t-\tau)$, γ is the damping coefficient, β and ν are the feedback gains, $\tau\geq 0$ is the time delay in the paths of displacement feedback and velocity feedback. ε and ω are the amplitude and frequency of the periodic signal. The $\eta(t)$ denotes a Gaussian colored noise with the following statistical properties:[12]

$$\langle\eta(t)\rangle=0,\ \langle\eta(t)\eta(s)\rangle=\frac{D}{\tau_1}\exp\left[-\frac{|t-s|}{\tau_1}\right],$$

where D is noise intensity and τ_1 is correlation time of the colored noise. The colored noise $\eta(t)$ in Eq. (1) can be obtained through a first-order low-pass filter by passing Gaussian white noise $W(t)$ as the following form:

$$\dot{\eta}(t)=-\frac{1}{\tau_1}\eta(t)+\frac{1}{\tau_1}W(t),$$

where $\langle W(t)\rangle=0$, $\langle W(t)W(s)\rangle=2D\delta(t-s)$. δ is the Dirac delta function.

The potential function $U_0(x)$ in Eq. (1) has the following form:

$$U_0(x)=\frac{h}{2}x^2-\frac{(1+h)b}{4}x^4+\frac{c}{6}x^6, \quad (2)$$

where the parameters b, c, h are positive. From Eq. (2), the equilibrium points of $U_0(x)$ are easily found

$$x_{mi}=\mp\sqrt{\frac{b(1+h)+\sqrt{b^2(1+h)^2-4hc}}{2c}}\ (i=1,3),\ x_{m2}=0,$$

$$x_{nj}=\mp\sqrt{\frac{b(1+h)-\sqrt{b^2(1+h)^2-4hc}}{2c}}\ (j=1,2),$$

where $(x_{mi},0)$ $(i=1,2,3)$ denote stable equilibrium points and $(x_{nj},0)$ $(j=1,2)$ denote unstable equilibrium points. In Fig. 1, $U_0(x)$ is plotted for fixed $h=1$, $b=0.9$, and $c=0.6$. It is seen that $U_0(x)$ has the triple-well potential structure.

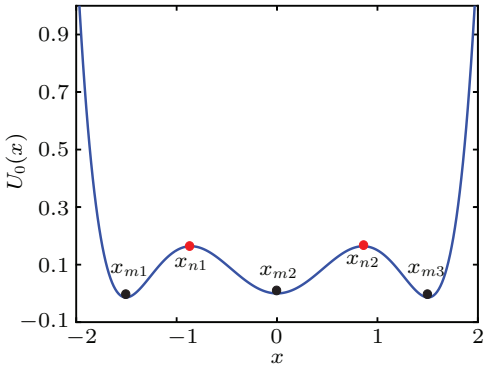


Fig. 1. The plot of potential function $U_0(x)$ with $h=1$, $b=0.9$, and $c=0.6$.

2.1. Stationary probability density

To obtain the SPD of Eq. (1), the generalized harmonic function is introduced and the system states can be expressed as

$$\begin{aligned}x(t)&=A(H(t))\cos[\omega(H(t))t+\varphi(t)]+x_{mi}[H(t)],\\ \dot{x}(t)&=-A(H(t))\omega(H(t))\sin[\omega(H(t))t+\varphi(t)],\end{aligned} \quad (3)$$

where $A(H)$ represents the energy-dependent amplitude, $\omega(H)$ denotes the energy-dependent frequency, $x_{mi}(H)$ $(i=1,2,3)$ represents the stable equilibrium points as displayed in Fig. 1.

Based on the transformation (3), the time-delayed displacement and velocity feedback control terms in Eq. (1) can be expressed approximately as

$$\begin{aligned}x(t-\tau)&\approx-\frac{\dot{x}(t)}{\omega(H(t))}\sin[\omega(H(t))\tau]+(x(t)-x_{mi}(H(t)))\\&\quad\times\cos[\omega(H(t))\tau],\\ \dot{x}(t-\tau)&\approx\dot{x}(t)\cos[\omega(H(t))\tau]+(x(t)-x_{mi}(H(t)))\,\omega(H(t))\\&\quad\times\sin[\omega(H(t))\tau].\end{aligned} \quad (4)$$

Substituting Eq. (4) into Eq. (1) leads to the following equation:

$$\ddot{x}+\tilde{\gamma}\dot{x}+\frac{\mathrm{d}U_0(x)}{\mathrm{d}x}+\tilde{\delta}(x-x_{mi})=\varepsilon\cos(\omega t)+\eta(t), \tag{5}$$

where

$$\begin{aligned}\tilde{\gamma}&=\gamma-\upsilon\cos(\omega(H)\tau)+\frac{\beta}{\omega(H)}\sin(\omega(H)\tau),\\ \tilde{\delta}&=-\beta\cos(\omega(H)\tau)-\upsilon\omega(H)\sin(\omega(H)\tau).\end{aligned} \tag{6}$$

According to Eq. (5), one can get the equivalent potential function and total energy function as

$$U(x)=\frac{1}{2}hx^2-\frac{1}{4}b(1+h)x^4+\frac{1}{6}cx^6+\frac{1}{2}\tilde{\delta}x^2, \tag{7}$$

$$H=\frac{1}{2}\dot{x}^2+U(x). \tag{8}$$

From Eqs. (5) and (6), it is seen that the $\omega(H)$ depends on the system energy (8). Thus, for a given energy level H, one can get the energy-dependent period

$$T(H)=\oint\frac{\mathrm{d}X}{\sqrt{2H-2U(X)}}$$

and the energy-dependent frequency $\omega(H)=2\pi/T(H)$ by the iteration method due to the existence of the unknown $\omega(H)$ in $U(X)$. That is,

$$\omega(H)=\frac{2\pi}{T(H)}=2\pi\left[\int_{x_1}^{x_2}\frac{\mathrm{d}x}{\sqrt{2H-2U(x)}}\right]^{-1}, \tag{9}$$

where the minimum and maximum vibrating displacements x_1 and x_2 are determined by equation $H=U(A)$ for the system without delayed states feedback.

Figure 2 shows the calculated total energy and different energy-dependent frequency for different steady states of potential function. At the three stable equilibrium points $(x_{m1},0)$, $(x_{m2},0)$, $(x_{m3},0)$, the total energy H reaches a local minimum while the energy-dependent frequency $\omega(H)$ exhibits a local maximum. It is observed that the local maximum of $\omega(H)$ at the left-side and right-side stable equilibrium point is larger than that at middle stable point.

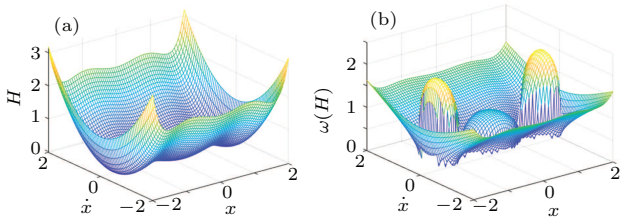


Fig. 2. (a) The total energy, (b) the energy-dependent frequency for the state variables of unperturbed and uncontrolled system. The parameters are chosen as $h=1$, $b=0.9$, and $c=0.6$.

According to Eq. (8), equation (5) can be rewritten as

$$\dot{x}=\pm\sqrt{2H-2U(x)}, \tag{10}$$

$$\dot{H}=-\dot{x}(\tilde{\gamma}\dot{x}-\tilde{\delta}x_{mi})+\dot{x}\eta(t)+\dot{x}\varepsilon\cos(\omega t). \tag{11}$$

Here $H(t)$ is an approximate Markovian process, then the Itô equation for the limiting diffusion process $H(t)$ can be expressed as

$$\mathrm{d}H=m(H)\mathrm{d}t+\sigma(H)\mathrm{d}B(t), \tag{12}$$

where $B(t)$ is a standard Wiener process, $m(H)$ and $\sigma(H)$ respectively represent the drift and diffusion coefficients

$$\begin{aligned}m(H)&=-\left\langle\dot{x}(\tilde{\gamma}\dot{x}-\tilde{\delta}x_{mi})\right\rangle_t+\frac{D}{1+\tau_1^2\omega^2(H)}+\langle\dot{x}\varepsilon\cos(\omega t)\rangle_t,\\ \sigma^2(H)&=\frac{2D}{1+\tau_1^2\omega^2(H)}\left\langle\dot{x}^2\right\rangle_t,\end{aligned} \tag{13}$$

where the time averaging

$$\langle\cdot\rangle_t=\frac{1}{T}\oint(\cdot)\mathrm{d}t=\frac{1}{T}\oint\frac{(\cdot)}{\dot{x}}\mathrm{d}x=\frac{\omega(H)}{2\pi}\oint\frac{(\cdot)}{\dot{x}}\mathrm{d}x.$$

The closed-loop integration is carried out corresponding to different energy levels. Especially, when the motion is moving in the right-side or left-side potential well, one has

$$\langle\dot{x}x_{mi}\rangle_t=\frac{1}{T}\oint x_{mi}\mathrm{d}x=\frac{1}{T_R+T_L}\left[\oint_R x_{m3}\mathrm{d}t+\oint_L x_{m1}\mathrm{d}t\right]=0.$$

Based on Eqs. (12) and (13), the SPD of the total energy $H(t)$ can be derived as

$$p(H)=\frac{N}{\sigma^2(H)}\exp\left[\int\frac{2m(H)}{\sigma^2(H)}\mathrm{d}H\right], \tag{14}$$

where the N is a normalization constant.

Considering the formula

$$\frac{\mathrm{d}}{\mathrm{d}H}\ln\left[T(H)\left\langle\dot{X}^2\right\rangle_t\right]=\frac{1}{\left\langle\dot{X}^2\right\rangle_t}$$

and Eq. (14), the joint SPD of system (5) can be obtained as

$$\begin{aligned}p(x,\dot{x})&=\frac{p(H)}{T(H)}\\ &=\frac{N(1+\tau_1^2\omega^2(H))}{D}\exp\left[-\frac{\tilde{\gamma}(1+\tau_1^2\omega^2(H))}{D}\right.\\ &\quad\times\left(\frac{1}{2}\dot{x}^2+\frac{1}{2}\left(h+\tilde{\delta}\right)x^2-\frac{1}{4}b(1+h)x^4\right.\\ &\quad\left.\left.+\frac{1}{6}cx^6-x\varepsilon\cos(\omega t)\right)\right].\end{aligned} \tag{15}$$

From Eq. (15), the expression of generalized potential function is given as

$$\begin{aligned}\tilde{U}(x,\dot{x},t)&=\tilde{\gamma}(1+\tau_1^2\omega^2(H))\left(\frac{1}{2}\dot{x}^2+\frac{1}{2}\left(h+\tilde{\delta}\right)x^2\right.\\ &\quad\left.-\frac{1}{4}b(1+h)x^4+\frac{1}{6}cx^6-x\varepsilon\cos(\omega t)\right).\end{aligned} \tag{16}$$

2.2. The effects of system parameters on SPD

It is shown that there is enough time for the tristable system to reach the local equilibrium point during the period of $1/\Omega$.[14] Thus, the effects of colored noise, damping coefficient, and delayed states feedback on the joint SPD (15) are analyzed as following by ignoring the periodic excitation (*i.e.*, $\varepsilon = 0$).

Figure 3 shows the effects of feedback gains and time delay on the joint SPD. In Fig. 3(a), the shape of the joint SPD displays a triple-peak structure, which indicates the system has a transition motion among three inter-wells. With the increase of displacement feedback gain β in Fig. 3(b), the middle peak of the joint SPD decreases while the peaks on left and right sides increase. That is, the system mainly performs a motion between the left and right potential well, whose dynamical behaviors are similar to those of bistable system. When the velocity feedback gain υ is increased, compared with that in Fig. 3(a), figure 3(c) shows the height of middle peak decreases slightly. When the time delay is increased in Fig. 3(d), the joint SPD is a trimodal structure with a uniform depth for the triple-well potentials. In a word, the time delay and feedback gains play an important role in the shapes of the joint SPD, which can be used to adjust the system structure for achieving the desired dynamics.

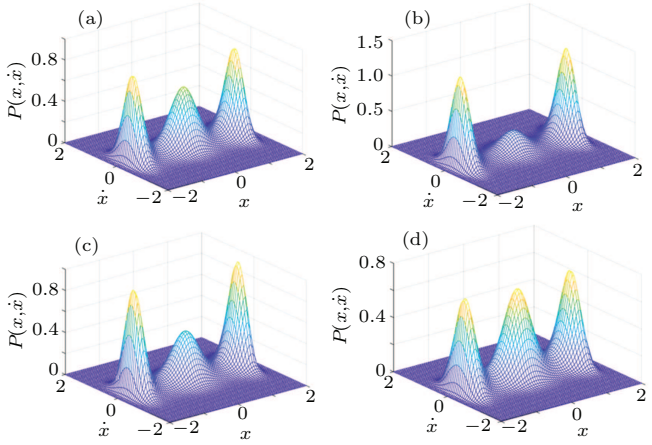


Fig. 3. The effects of feedback gains and time delay on the joint SPD: (a) $\beta = 0.01$, $\upsilon = 0.01$, $\tau = 0.1$; (b) $\beta = 0.1$, $\upsilon = 0.01$, $\tau = 0.1$; (c) $\beta = 0.01$, $\upsilon = 0.1$, $\tau = 0.1$; (d) $\beta = 0.01$, $\upsilon = 0.01$, $\tau = 1.5$. The other parameters are chosen as $c = 0.6$, $\tau_1 = 0.1$, $D = 0.1$, $\gamma = 1$.

The plots of joint SPD with different noise intensity, noise correlation time, and damping coefficient are demonstrated in Fig. 4. The following conclusions are obtained mainly by comparing with Fig. 3(a). From Fig. 4(a), it is seen that the increase of correlation time τ_1 results in the decrease of middle peak in joint SPD. The system spends most time in the left and right sides potential wells. In Fig. 4(b), the heights of three peaks in joint SPD tend to the same as the noise intensity D increases. That is, noise intensity of colored noise can strengthen the inter-well transition. Figure 4(c) shows that the decrease of damping coefficient γ leads to a trimodal structure with a uniform depth for the tristable potentials. This phenomenon is in line with the physical intuition because the particles are increased their energy very rapidly and released from the potential wells for small damping coefficient. To verify the theoretical result (15), the MCS of Eq. (1) with the same parameters as Fig. 4(c) is given in Fig. 4(d). It is obvious that the theoretical and numerical results coincide very well.

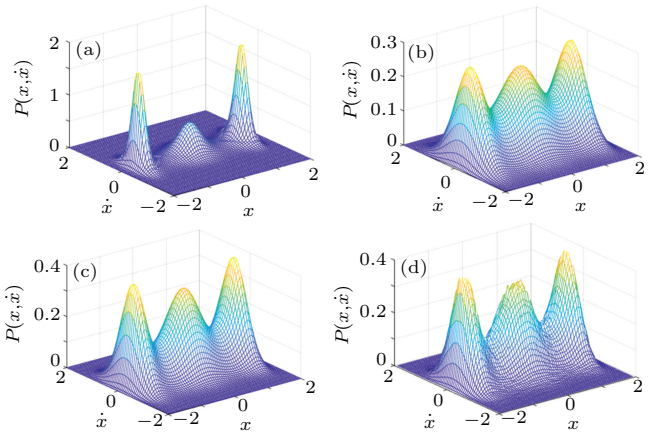


Fig. 4. The effects of colored noise and damping coefficient on the joint SPD: (a) $\tau_1 = 0.5$, $D = 0.1$, $\gamma = 1$; (b) $D = 0.3$, $\tau_1 = 0.1$, $\gamma = 1$; (c) $\gamma = 0.5$, $\tau_1 = 0.1$, $D = 0.1$; (d) MCS result for the same parameters as those in panel (c). The other parameters are chosen as $c = 0.6$, $\beta = 0.01$, $\upsilon = 0.01$.

3. Stochastic resonance

Based on the generalized potential function (16) and the linear response theory, the analytical expression of the spectral amplification will be derived and the influents of system parameters on SR will be discussed in the following subsections.

3.1. Spectral amplification

Let $\dot{x} = y$, equation (5) can be rewritten as

$$\begin{cases} \dot{x} = y, \\ \dot{y} = -\tilde{\gamma} y - hx + b(1+h)x^3 - cx^5 - \tilde{\delta}(x - x_{mi}) \\ \quad\quad + \eta(t) + \varepsilon\cos(\omega t). \end{cases} \tag{17}$$

Equation (17) can be considered as a discrete-state Markov process describing the transfer of probability masses p_i $(i = 1,2,3)$ within the adiabatic approximation. The corresponding master equation is derived as

$$\frac{\mathrm{d}\boldsymbol{P}}{\mathrm{d}t} = \boldsymbol{W}\boldsymbol{P}, \tag{18}$$

where $\boldsymbol{P} = \left[\, p_1 \;\; p_2 \;\; p_3 \,\right]^{\mathrm{T}}$ and the superscript T denotes the transpose of matrix. The transfer matrix $\boldsymbol{W}$ has the following form:

$$\boldsymbol{W} = \begin{bmatrix} -k_{1,2} & k_{2,1} & 0 \\ k_{1,2} & -(k_{2,1} + k_{2,3}) & k_{3,2} \\ 0 & k_{2,3} & -k_{3,2} \end{bmatrix}, \tag{19}$$

in which

$$k_{1,2} = \frac{1}{2\pi}\sqrt{\frac{\lambda_{m1}^{+}\lambda_{m1}^{-}\lambda_{n1}^{+}}{|\lambda_{n1}^{-}|}} \times \exp\left\{\frac{\tilde{U}(x_{m1},0,t)-\tilde{U}(x_{n1},0,t)}{D}\right\}, \quad (20)$$

$$k_{2,1} = \frac{1}{2\pi}\sqrt{\frac{\lambda_{m2}^{+}\lambda_{m2}^{-}\lambda_{n1}^{+}}{|\lambda_{n1}^{-}|}} \times \exp\left\{\frac{\tilde{U}(x_{m2},0,t)-\tilde{U}(x_{n1},0,t)}{D}\right\}, \quad (21)$$

$$k_{2,3} = \frac{1}{2\pi}\sqrt{\frac{\lambda_{m2}^{+}\lambda_{m2}^{-}\lambda_{n2}^{+}}{|\lambda_{n2}^{-}|}} \times \exp\left\{\frac{\tilde{U}(x_{m3},0,t)-\tilde{U}(x_{n2},0,t)}{D}\right\}, \quad (22)$$

$$k_{3,2} = \frac{1}{2\pi}\sqrt{\frac{\lambda_{m3}^{+}\lambda_{m3}^{-}\lambda_{n2}^{+}}{|\lambda_{n2}^{-}|}} \times \exp\left\{\frac{\tilde{U}(x_{m3},0,t)-\tilde{U}(x_{n2},0,t)}{D}\right\}. \quad (23)$$

The expressions of $\lambda_{mi}^{\pm}$ $(i=1,2,3)$ and $\lambda_{nj}^{\pm}$ $(j=1,2)$ in Eqs. (20)–(23) can be determined by

$$\lambda_{mi}^{\pm} = \frac{-\tilde{\gamma}\pm\sqrt{\tilde{\gamma}^2+4\left(-h+3b(1+h)x_{mi}^2-5cx_{mi}^4\right)}}{2}, \quad (i=1,2,3), \quad (24)$$

$$\lambda_{ni}^{\pm} = \frac{-\tilde{\gamma}\pm\sqrt{\tilde{\gamma}^2+4\left(-h+3b(1+h)x_{ni}^2-5cx_{ni}^4\right)}}{2}, \quad (i=1,2), \quad (25)$$

where the $\lambda_{mi}^{\pm}$ $(i=1,2,3)$ are eigenvalues of the linearization matrix of Eq. (17) on stable states $(x_{mi},0)$ $(i=1,2,3)$ and the $\lambda_{nj}^{\pm}$ $(j=1,2)$ are eigenvalues of the linearization matrix of Eq. (17) on unstable points $(x_{nj},0)$ $(j=1,2)$.

For the small signal amplitude ε, the first-order approximation of $\boldsymbol{P}$ can be expressed as

$$p_i = p_i^0 + \varepsilon\Delta p_i, \quad (i=1,2,3), \quad (26)$$

where Δp_i is the first-order correction to p_i.

Expanding the transfer matrix $\boldsymbol{W} = \boldsymbol{W}^0 + \varepsilon\Delta\boldsymbol{W}\cos\omega t$ and substituting Eq. (26) into Eq. (18) leads to the following expressions:

$$\begin{cases} \dfrac{\mathrm{d}p_i^0}{\mathrm{d}t} = \sum\limits_{l=1}^{3}\boldsymbol{W}_{il}^0 p_l^0, \\ \dfrac{\mathrm{d}\Delta p_i}{\mathrm{d}t} = \sum\limits_{l=1}^{3}\boldsymbol{W}_{il}^0\Delta p_i + \sigma_i^0\cos(\omega t), \end{cases} \quad (27)$$

where $\boldsymbol{W}^0$ and p_i^0 $(i=1,2,3)$ are the transition rate matrix and probability for system without periodic signal, respectively. The $\boldsymbol{W}_{il}^0$ $(i=1,2,3;\ l=1,2,3)$ are the corresponding element of matrix $\boldsymbol{W}^0$ and the σ_i^0 $(i=1,2,3)$ are the element of three-dimensional column vector $\boldsymbol{\sigma}^0$. That is,

$$\boldsymbol{\sigma}^0 = \frac{\tilde{\gamma}\left(1+\tau_1^2\omega^2(H)\right)}{D}\begin{bmatrix} -k_{1,2}^0(x_{n1}-x_{m1})p_1^0 + k_{2,1}^0(x_{n1}-x_{m2})p_2^0 \\ k_{1,2}^0(x_{n1}-x_{m1})p_1^0 - \left[k_{2,1}^0(x_{n1}-x_{m2})+k_{2,3}^0(x_{n2}-x_{m2})\right]p_2^0 + k_{3,2}^0(x_{n2}-x_{m3})p_3^0 \\ k_{2,3}^0(x_{n2}-x_{m2})p_2^0 - k_{3,2}^0(x_{n2}-x_{m3})p_3^0 \end{bmatrix}.$$

The solution of Eq. (27) has the following form for considering the limit of long time:

$$\Delta p_i = q_i\sin(\omega t) + w_i\cos(\omega t). \quad (28)$$

Substituting Eq. (28) into Eq. (27), one has

$$q_i = \sum_{k=1}^{3}\omega(\kappa_k^2+\omega^2)^{-1}\alpha_k\zeta_{k,i},$$

$$w_i = -\sum_{k=1}^{3}\kappa_k(\kappa_k^2+\omega^2)^{-1}\alpha_k\zeta_{k,i},$$

where κ_k and ζ_k are the eigenvalues and the eigenvectors of $\boldsymbol{W}^0$, respectively. The α_k $(k=1,2,3)$ are the expansion coefficients of vector $\boldsymbol{\sigma}^0$ of Eq. (27) in the basis of ζ_k. In general, $\boldsymbol{\sigma}^0$ can be expressed as

$$\boldsymbol{\sigma}^0 = \sum_{k=1}^{3}\alpha_k\zeta_k.$$

According to Eq. (28), the steady-state response of system (17) can be derived as follows:

$$\langle x(t)\rangle = \varepsilon\sum_{i=1}^{3}x_{mi}\left[q_i\sin(\omega t)+w_i\cos(\omega t)\right] = V\cos(\omega t+\theta). \quad (29)$$

Based on Eq. (29), the spectral amplification $\eta = (V/\varepsilon)^2$ is obtained as

$$\eta = \left[\sum_{i=1}^{3}\sum_{k=1}^{3}x_{mi}\omega(\kappa_k^2+\omega^2)^{-1}\alpha_k\zeta_{k,i}\right]^2 + \left[\sum_{i=1}^{3}\sum_{k=1}^{3}x_{mi}\kappa_k(\kappa_k^2+\omega^2)^{-1}\alpha_k\zeta_{k,i}\right]^2. \quad (30)$$

In the following analysis, the spectral amplification η is used to characteristic the SR phenomenon when the plot of η displays a non-monotonic behavior *versus* noise intensity.

3.2. The effects of system parameters on SR

The effects of time delay and feedback gains on the spectral amplification η and SR are shown in Fig. 5. In Fig. 5, the curves of η *versus* D show a single-peak structure and the SR phenomenon is observed. In Figs. 5(a) and 5(b), the curves of η are plotted for the case of time-delayed displacement feedback and time-delayed velocity feedback respectively. For both cases, the maximum peak value of η appears in the system with negative feedback gain, which means that the negative feedback gain tends to strengthen SR phenomenon for fixed τ. However, the SR effect for positive feedback gain case is even worse than that without feedback control as shown in Figs. 5(a) and 5(b). Figures 5(c) and 5(d) display the effects of time delay on SR in the system with displacement and velocity delayed states feedback. A comparison between Figs. 5(c)–5(d) and 5(a)–5(b) illustrates that the value of resonant peak increases when both displacement and velocity time-delayed feedback control are considered. With the increase of τ, the SR peak increases for negative velocity feedback gain (*i.e.*, $\upsilon < 0$); while it decreases with increasing τ for positive velocity feedback gain (*i.e.*, $\upsilon > 0$). In other words, the SR effect and control performance can be enhanced by choosing appropriate combination of time delay and feedback gain.

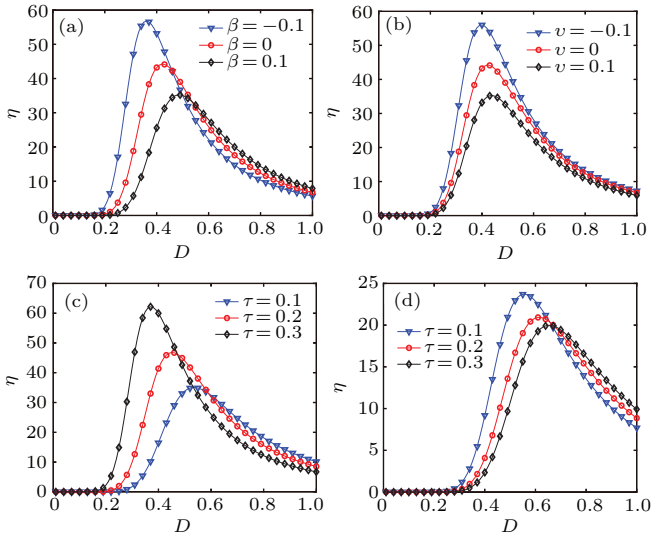


Fig. 5. The spectral amplification η *versus* noise intensity D with different values of β, υ, and τ: (a) $\upsilon = 0$, $\tau = 0.1$; (b) $\beta = 0$, $\tau = 0.1$; (c) $\beta = 0.2$, $\upsilon = -0.1$; (d) $\beta = 0.2$, $\upsilon = 0.1$. The other parameters are chosen as $c = 0.4$, $\tau_1 = 0.1$, $\gamma = 1$.

Figure 6 depicts the curves of the spectral amplification η as a function of noise intensity D for different correlation time and damping coefficient. It is observed that the curve exhibits a maximum at the optimal noise intensity, where the SR appears. From Fig. 6(a), the peak value is decreased while the optimal noise intensity increases with increasing correlation time of noise. That is, the SR effect is suppressed by correlation time. In Fig. 6(b), the increasing damping coefficient decreases the SR peak value and increases the optimal noise intensity. This phenomenon can be understood as the big damping hinders the system from transiting among the potential wells. Thus, the system needs to overcome this hinderance by increasing the noise intensity.

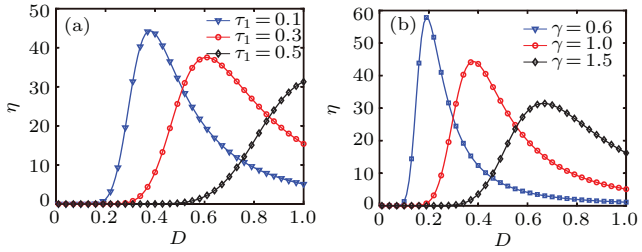


Fig. 6. The spectral amplification η *versus* noise intensity D with different values of τ_1 and γ: (a) $\gamma = 1$; (b) $\tau_1 = 0.1$. The other parameters are chosen as $c = 0.4$, $\beta = -0.1$, $\upsilon = 0.1$, $\tau = 0.1$.

4. Conclusions

In this paper, the displacement and velocity delayed states feedback are considered in an underdamped tri-stable model, which is driven by colored noise and a periodic signal. To explore the SR phenomenon, the stochastic averaging based on energy-dependent frequency is proposed to tackle the theoretical treatment of SR in the SDDE. The analytical expressions for SPD and spectral amplification are derived. The effects of noise intensity, damping coefficient and time-delayed feedback on SPD are discussed. It is found that the shape of joint SPD depends on the time delay, feedback gains and correlation time. Especially, the joint SPD is a trimodal structure with a uniform depth by choosing proper time delay and feedback gains. At the optimal noise intensity, the curve of spectral amplification shows a single-peak structure and SR phenomenon is observed. When the time delay increases, the SR peak increases for negative velocity feedback gain and decreases for positive velocity feedback gain. That is, the SR effect and control performance can be improved through adjusting time delay and feedback gains.

In practice, numerous physical systems are subjected to randomly fluctuating excitation and time delay. The obtained results provide the reliable basis for studying the other noise-induced behaviors in the tri-stable dynamical model with time-delayed feedback, such as coherence resonance and stochastic bifurcation. Furthermore, multi-stable characteristics are usually encountered in some physical devices and mathematical models.

Acknowledgements

Project supported by the National Natural Science Foundation of China (Grant No. 12072025) and the Beijing Natural

Science Foundation (Grant No. 1222015).

References

[1] Gammaitoni L, Hanggi P, Jung P and Marchesoni F 1998 *Rev. Mod. Phys.* **70** 223
[2] Hu G, Ditzinger T, Ning C Z and Haken H 1993 *Phys. Rev. Lett.* **71** 807
[3] Douglass J K, Wilkens L, Pantazelou E and Moss F 1993 *Nature* **365** 337
[4] Zhou T and Moss F 1990 *Phys. Rev. A* **41** 4255
[5] Kenfack A and Singh K P 2010 *Phys. Rev. E* **82** 046224
[6] Yang T T, Zhang H Q, Xu Y and Xu W 2014 *Int. J. Nonlinear Mech.* **67** 42
[7] Laas K, Mankin R and Rekker A 2009 *Phys. Rev. E* **79** 051128
[8] Jin Y F 2018 *Chin. Phys. B* **27** 050501
[9] Jin Y F, Ma Z M and Xiao S M 2017 *Chaos, Solitons & Fractals* **103** 470
[10] Liu R N and Kang Y M 2018 *Phys. Lett. A* **382** 1656
[11] Ding Y M, Kang Y M and Zhai Y J 2023 *IEEE Transactions on Instrumentation and Measurement* **72** 3510812
[12] Zhang T T, Jin Y F and Zhang Y X 2023 *J. Sound Vib.* **543** 117379
[13] Zhou S X, Cao J Y, Inman D J, Lin J and Li D 2016 *J. Sound Vib.* **373** 223
[14] Zhou B L, Jin Y F and Xu H D 2022 *Appl. Math. Model.* **108** 427
[15] Melancon D, Gorissen B, Garcia-Mora C J, Hoberman C and Bertoldi K 2021 *Nature* **592** 545
[16] Jin Y F and Wang H Q 2020 *Chaos, Solitons & Fractals* **133** 109633
[17] Masoller C 2002 *Phys. Rev. Lett.* **88** 034102
[18] Martínez-Zérega B E and Pisarchik A N 2012 *Commun. Nonlinear Sci. Numer. Simulat.* **17** 4023
[19] Kraut S and Feudel U 2002 *Phys. Rev. E* **66** 015207
[20] Nicolis C 2010 *Phys. Rev. E* **82** 011139
[21] Nicolis G and Nicolis C 2016 *Entropy* **18** 172
[22] Xu P F and Jin Y F 2020 *Chaos, Solitons & Fractals* **138** 109857
[23] Jin Y F and Wang H Q 2021 *Chin. J. Theor. Appl. Mech.* **53** 865
[24] Zhang H Q, Xu Y, Xu W and Li X C 2012 *Chaos* **22** 043130
[25] Arathi S and Rajasekar S 2011 *Phys. Scr.* **84** 065011
[26] Jin Y F, Wang H T, Xu P F and Xie W X 2023 *Probabilist. Eng. Mech.* **72** 103418
[27] Pyragas K 1992 *Phys. Lett. A* **170** 421
[28] Just W, Bernard T, Ostheimer M, Reibold E and Benner H 1997 *Phys. Rev. Lett.* **78** 203
[29] Hu H Y and Wang Z H 1998 *J. Sound Vibr* **214** 213
[30] Guillouzic S, L'Heureux I and Longtin A 1999 *Phys. Rev. E* **59** 3970
[31] Elbeyli O, Sun J Q and Unal G 2005 *Commun. Nonlinear Sci.* **10** 85
[32] Tsimring L S and Pikovsky A 2001 *Phys. Rev. Lett.* **87** 250602
[33] Jin Y F 2012 *Physica A* **391** 1928
[34] Jin Y F, Wang H T and Xu P F 2023 *Chaos, Solitons & Fractals* **168** 113099
[35] Xu P F, Jin Y F and Xiao S M 2017 *Chaos* **27** 113109
[36] Li W J, Ren L H and Duan F B 2022 *Chin. Phys. B* **31** 080503